

This document contains a pre-print version of the paper

Bifurcation suppression in regenerative amplifiers by active feedback methods

authored by A. Deutschmann, T. Flöry, K. Schrom, V. Stummer, A. Baltuška, and A. Kugi
and published in *Optics Express*.

The content of this pre-print version is identical to the published paper but without the publisher's final layout or copy editing. Please, scroll down for the article.

Cite this article as:

A. Deutschmann, T. Flöry, K. Schrom, V. Stummer, A. Baltuška, and A. Kugi, "Bifurcation suppression in regenerative amplifiers by active feedback methods", *Optics Express*, vol. 27, no. 26, 2019. DOI: [10.1364/OE.380404](https://doi.org/10.1364/OE.380404)

BibTex entry:

```
@ARTICLE{Deutschmann19,  
  author = {Deutschmann, A. and Fl\"ory, T. and Schrom, K. and Stummer, V. and Baltu\v{s}ka, A. and Kugi, A  
    .},  
  title = {Bifurcation suppression in regenerative amplifiers by active feedback methods},  
  journal = {Optics Express},  
  year = 2019,  
  volume = 27,  
  number = 26,  
  doi = {10.1364/OE.380404}  
}
```

Link to original paper:

<http://dx.doi.org/10.1364/OE.380404>

Read more ACIN papers or get this document:

<http://www.acin.tuwien.ac.at/literature>

Contact:

Automation and Control Institute (ACIN)
Vienna University of Technology
Gusshausstrasse 27-29/E376
1040 Vienna, Austria

Internet: www.acin.tuwien.ac.at
E-mail: office@acin.tuwien.ac.at
Phone: +43 1 58801 37601
Fax: +43 1 58801 37699

Bifurcation suppression in regenerative amplifiers by active feedback methods

Andreas Deutschmann,^{1,*} Tobias Flöry,² Katharina Schrom,¹
Vinzenz Stummer,² Andrius Baltuška,² and Andreas Kugi¹

¹Automation and Control Institute (ACIN), Complex Dynamical Systems Group, TU Wien, Vienna, Austria

²Photonics Institute, Ultrafast Laser Group, TU Wien, Vienna, Austria

*deutschmann@acin.tuwien.ac.at

Abstract: The performance of regenerative amplifiers at high repetition rates is often limited by the occurrence of bifurcations induced by a destabilization of the pulse-to-pulse dynamics. While bifurcations can be suppressed by increasing the seed energy using dedicated pre-amplifiers, the availability of adjustable filters and control electronics in modern pulse amplifiers allows to exploit feedback strategies to cope with these instabilities. In this paper, we present a theoretical and experimental analysis of active feedback methods to stabilize otherwise unstable operational regimes of regenerative amplifiers. To this end, the dynamics of regenerative amplifiers are investigated starting from a general space-dependent description to obtain a generalization of existing models from the literature. Suitable feedback strategies are then developed utilizing measurements of the output pulse energies or the transmitted pump light, respectively. The effectiveness of the proposed approach is highlighted by experimental results for a Yb:CaF₂-based regenerative amplifier.

© 2019 Optical Society of America under the terms of the OSA Open Access Publishing Agreement

1. Introduction

Regenerative amplifiers (RAs) are a widely used tool for the generation of high-intensity laser pulses. Combined with chirped pulse amplification techniques to reduce the B-integral and avoid amplifier optical damage, RAs are used to create ultra-fast high energy pulses with a wide range of potential applications such as strong field physics [1], coherent control [2], and ablation-based material processing [3] including various medical applications. Although high repetition rates are considered beneficial for several applications [4], RAs are known to become unstable quite easily for a range of repetition rates around the inverse life time of the laser medium's upper lasing energy level [5]. When operated within the unstable region, the sequence of output pulses either converges to a periodic orbit whereby the limit set exhibits so-called period-doubling bifurcations or remains aperiodic in the case of deterministic chaos. While it is always possible to find stable operating points at a desired repetition rate, the operating points with highest power output and highest energy efficiency are typically located in the vicinity of the unstable region.

As a result, this topic has been of significant scientific interest since the first experimental results were documented in [6]. A numerical study using a simple rate equation model in [4] highlights the coupling mechanism of subsequent pulses that leads to period-doubling bifurcations and ultimately deterministic chaos. By using analytic solutions of the rate equation model under quite restrictive assumptions, a detailed parameter study of the underlying problem in [7] and [8] finally shows that the bifurcations can be suppressed by increasing the seed energy. Although this requires a dedicated pre-amplifier, it has become the standard approach today. Recently, there

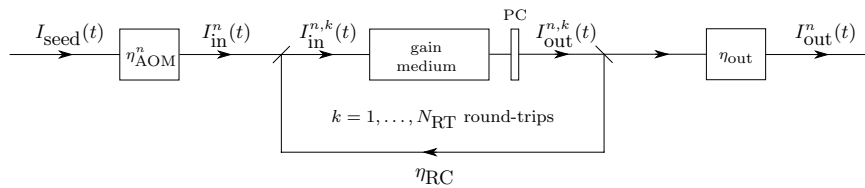


Fig. 1. Schematic overview of a RA with adjustable input loss factor η_{AOM}^n .

have been attempts to avoid the bifurcation regime by saturating the gain medium and thus operating the amplifier beyond the unstable region [9]. Since this may result in extremely high transient pulse energies, it requires a careful design of the RA to avoid pulses above the damage threshold of the optics in the cavity. Alternatively, operation at a specifically chosen limit cycle and picking the desired pulses from the amplified pulse train afterwards is suggested in [10].

By increasing the seed energy in a saturating amplifier as proposed in [8], one effectively reduces the total gain, which is clearly beneficial for the amplifier’s stability properties as it is also known from electronic amplifiers. However, circuit engineers developed another highly successful and far-reaching strategy to cope with emerging instabilities in high-gain amplifiers: feedback. In fact, [4] already points to the possibility of active stabilization techniques. Since many amplifiers already utilize controllable input filters to compensate for effects such as gain narrowing or nonlinear phase distortions [11–15], it seems natural to investigate strategies to stabilize the amplifier’s dynamics by modulating the energy of the seed pulses. While simple feedback schemes are commonly employed in CW lasers or Q-switched lasers to statically compensate for external disturbances, the authors are not aware of any applications of feedback to actively modify the dynamics of RAs.

In this paper, we present active feedback methods to stabilize otherwise unstable operational regimes of RAs and thus suppress bifurcations of the uncontrolled amplifier. To this end, we will start with a general space-dependent mathematical model of regenerative amplifiers and show that a detailed description of the amplifier’s pulse-to-pulse dynamics for different levels of (continuous) pumping can be systematically derived based on mild assumptions only. The resulting discrete-time dynamic model can be considered a generalization of the model used in [7]. Using this description, two feedback approaches will be developed that utilize measurements of the output pulse energy or the residual pumping beam, respectively. Finally, the validity of the proposed feedback strategy is highlighted by experimental results.

2. Dynamics of regenerative amplifiers

In case the spectral properties of the pulse amplification process can be neglected, instead of using the rather complex Maxwell-Bloch equations, the laser light is usually treated as a transport process of monochromatic photons conveying no additional phase information described by the intensity I known as Frantz-Nodvik model [16]. For simplicity, we will focus on the case of a RA using a ring cavity design as shown in Fig. 1, although the proposed approach can be directly transferred to linear cavities. Thus, identical seed pulses $I_{\text{seed}}(t)$ from a source with repetition rate f_{rep} pass some kind of modulation device that allows to adjust the amount of additional spectrally homogeneous damping for each individual seed pulse. Using an acousto-optic modulator (AOM) with an adjustable

loss factor η_{AOM}^n , the resulting input pulse $I_{\text{in}}^n(t)$ is given by

$$I_{\text{in}}^n(t) = \eta_{\text{AOM}}^n I_{\text{seed}}(t). \quad (1)$$

It is assumed that further injection losses are already included in $I_{\text{seed}}(t)$ and thus $0 \leq \eta_{\text{AOM}}^n \leq 1$. The resulting pulse $I_{\text{in}}^n(t)$ is then injected into the resonator cavity with concentrated losses η_{RC} , whereby the k -th round-trip of the n -th input and output pulse is denoted by $I_{\text{in}}^{n,k}(t)$ and $I_{\text{out}}^{n,k}(t)$, respectively. The final amplified pulse after N_{RT} round-trips is then released by switching the Pockel's cell (PC) and all losses due to the pulse extraction are again subsumed in η_{out} , i.e.,

$$I_{\text{out}}^n(t) = \eta_{\text{out}} I_{\text{out}}^{n,N_{\text{RT}}}(t). \quad (2)$$

To describe the amplification and regeneration process, we assume that the gain medium is operated in a so-called end-pumped configuration, i.e. that the continuous pumping beam is fed through the crystal axially aligned with the laser beam and in the same direction of propagation. Additionally, we assume that the transversal intensity profile of the pulses and the pumping beam is homogeneous over a diameter d and zero outside. Aligning the propagation direction with the z -axis and assuming a homogeneously broadened quasi-three-level medium with the population inversion $\Delta N = N_2 - N_1$ of the lasing transition, the interaction of the pulse I and the pumping beam I_{P} during each round trip can be described by [17]

$$\frac{\partial I}{\partial t} + v \frac{\partial I}{\partial z} = \sigma v (f_1 + f_2) \Delta N I \quad (3a)$$

$$\frac{\partial I_{\text{P}}}{\partial t} + v_{\text{P}} \frac{\partial I_{\text{P}}}{\partial z} = -\sigma_{\text{P}} v_{\text{P}} \frac{(f_0 f_2 - f_3 f_1) N_{\text{dop}} - (f_0 + f_3) \Delta N}{f_1 + f_2} I_{\text{P}} \quad (3b)$$

$$\begin{aligned} \frac{\partial \Delta N}{\partial t} = & -\gamma_{21} f_2 (f_1 N_{\text{dop}} + \Delta N) - \frac{\sigma I}{\hbar \omega} (f_1 + f_2) \Delta N \\ & + \frac{\sigma_{\text{P}} I_{\text{P}}}{\hbar \omega_{\text{P}}} ((f_0 f_2 - f_3 f_1) N_{\text{dop}} - (f_0 + f_3) \Delta N), \end{aligned} \quad (3c)$$

with the relative occupancy factors f_i of the i -th energy level, the remaining relaxation rate of excited populations γ_{21} , the density of the dopant N_{dop} and the associated group velocities v , v_{P} , the transition cross-sections σ , σ_{P} and the angular frequencies ω , ω_{P} , respectively. Note that the simpler results for the case of a four-level material can be retrieved by setting $f_0 = f_2 = 1$ and $f_1 = f_3 = 0$.

2.1. Amplification during a single pass

For a single pass of the laser pulse through the laser material, the influence of the comparatively weak pumping beam and the relaxation of the excited populations via γ_{21} can be neglected due to the extremely short time scales. Applying these assumptions to (3) and transforming the equations onto a time frame $t \mapsto t - z/v$ travelling with the pulse, one obtains

$$\frac{\partial I}{\partial z} = \sigma (f_1 + f_2) \Delta N I \quad (4a)$$

$$\frac{\partial \Delta N}{\partial t} = -\frac{\sigma I}{\hbar \omega} (f_1 + f_2) \Delta N, \quad (4b)$$

with a generic input pulse at the left boundary $I(0, t) = I_{\text{in}}(t)$ and the initial density of the population inversion $\Delta N(z, 0) = \Delta N_{\text{in}}(z)$. The desired output pulse at the opposite

boundary $z = L$ is given by $I_{\text{out}}(t) = I(L, t)$ where L denotes the length of the laser medium. The remaining population inversion after the pulse has completely passed through the laser medium is denoted by $\Delta N_{\text{out}}(z)$. By introducing the time-varying gain $G(t)$ and the normalized fluence $H(t)$

$$G(t) = \exp \left(\sigma(f_1 + f_2) \int_0^L \Delta N(z, t) dz \right) \quad (5a)$$

$$H_{\text{in/out}}(t) = \frac{\sigma(f_1 + f_2)}{\hbar\omega} \int_0^t I_{\text{in/out}}(\xi) d\xi, \quad (5b)$$

equation (4) can be solved analytically [16, 17] to obtain the simple results

$$\ln \left(\frac{1 - \frac{1}{G(0)}}{1 - \frac{1}{G(t)}} \right) = H_{\text{in}}(t) \quad \text{and} \quad \ln \left(\frac{G(0) - 1}{G(t) - 1} \right) = H_{\text{out}}(t). \quad (6)$$

Using the remaining gain G_{out} after the pulse has passed and the total normalized fluence of the input and output pulses $H_{\text{in/out}}$, these relations can be written as

$$G_{\text{out}} = f_{\text{dep}}(G_{\text{in}}, H_{\text{in}}) = \frac{G_{\text{in}}}{G_{\text{in}} - (G_{\text{in}} - 1) \exp(-H_{\text{in}})} \quad (7a)$$

$$H_{\text{out}} = f_{\text{gain}}(G_{\text{in}}, H_{\text{in}}) = \ln [G_{\text{in}} \exp(H_{\text{in}}) - G_{\text{in}} + 1] \quad (7b)$$

linking the initial gain $G_{\text{in}} = G(0) = \exp \left(\sigma(f_1 + f_2) \int_0^L \Delta N_{\text{in}}(z) dz \right)$ and the total input fluence H_{in} with the remaining gain G_{out} and the corresponding total fluence H_{out} of the amplified pulse.

2.2. Gain restoration due to pumping

Now that a simple expression for the pulse amplification and the resulting saturation of the available gain has been found, a compatible description of the gain restoration due to the pumping process of duration $\Delta t = 1/f_{\text{rep}}$ shall be derived. Since no laser pulse is present during the regeneration periods (i.e., $I(z, t) = 0$), the full set of equations (3) can be rewritten as

$$\frac{1}{v_P} \frac{\partial I_P}{\partial t} = -\frac{\partial I_P}{\partial z} - \sigma_P \frac{(f_0 f_2 - f_3 f_1) N_{\text{dop}} - (f_0 + f_3) \Delta N}{f_1 + f_2} I_P \quad (8a)$$

$$\frac{\partial \Delta N}{\partial t} = -\gamma_{21} f_2 (f_1 N_{\text{dop}} + \Delta N) + \frac{\sigma_P I_P}{\hbar\omega_P} ((f_0 f_2 - f_3 f_1) N_{\text{dop}} - (f_0 + f_3) \Delta N), \quad (8b)$$

with the initial condition $\Delta N(z, 0) = \Delta N_{\text{in}}(z)$ using some arbitrary initial population inversion $\Delta N_{\text{in}}(z)$ and the boundary condition $I_P(0, t) = I_0(t)$. Here, $I_0(t)$ denotes the intensity of the pumping beam that is linked to the optical pump power $P_{\text{pump}}(t)$ by $I_0(t) = \frac{P_{\text{pump}}(t)}{A_B}$ with the beam's cross sectional area A_B . Additionally, the transport equation (8a) would require an initial condition for the intensity distribution $I_P(z, 0)$. Since the pump power $P_{\text{pump}}(t)$ and thus $I_0(t)$ varies slowly compared to the group velocity v_P , i.e., $\frac{1}{I_0(t)} \frac{\partial I_0(t)}{\partial t} \ll \frac{v_P}{L}$, the transport equation (8a) can be considered stationary as any perturbation to its steady state propagates through the laser rod extremely fast. Thus, applying singular perturbation theory (i.e., $v_P \rightarrow \infty$), one obtains

$$\frac{\partial I_P}{\partial z} = -\sigma_P \frac{(f_0 f_2 - f_3 f_1) N_{\text{dop}} - (f_0 + f_3) \Delta N}{f_1 + f_2} I_P \quad (9a)$$

$$\frac{\partial \Delta N}{\partial t} = -\gamma_{21} f_2 (f_1 N_{\text{dop}} + \Delta N) + \frac{\sigma_P I_P}{\hbar\omega_P} ((f_0 f_2 - f_3 f_1) N_{\text{dop}} - (f_0 + f_3) \Delta N). \quad (9b)$$

Proceeding as in the previous section by solving (9) and reformulating the result in terms of $G(t)$ according to (5a) using $\kappa_1 = \frac{f_0 f_2 - f_1 f_3}{f_1 + f_2}$ and $\kappa_2 = \frac{f_0 + f_3}{f_1 + f_2}$ yields

$$\begin{aligned} \frac{d}{dt} G(t) = & -\gamma_{21} f_2 [\sigma f_1 (f_1 + f_2) N_{\text{dop}} L + \ln(G(t))] G(t) \\ & + \sigma \frac{P_{\text{pump}}(t)}{A_B} \frac{(f_1 + f_2)^2}{\hbar \omega_P} \left[1 - \exp(-\sigma_P (\kappa_1 N_{\text{dop}} L)) G(t)^{\frac{\kappa_2 \sigma_P}{(f_1 + f_2) \sigma}} \right] G(t), \end{aligned} \quad (10)$$

with the initial condition $G(0) = \exp\left(\sigma(f_1 + f_2) \int_0^L \Delta N_{\text{in}}(z) dz\right) = G_{\text{in}}$. Thus, the gain after the regeneration period is given by $G_{\text{out}} = G(\Delta t)$. For convenience, we introduce the nomenclature

$$G_{\text{out}} = f_{\text{pump}}(G_{\text{in}}, P_{\text{pump}}(t)) \quad (11)$$

analogous to the previous section to describe the connection between G_{in} and G_{out} as a solution to (10) for a given $P_{\text{pump}}(t)$.

2.3. Discrete-time dynamical model

Using the solution of a single pass through the laser medium according to (7) and considering the losses in the cavity, one can write the effect of a single round-trip according to Fig. 1 as

$$\begin{bmatrix} G^{n,k+1} \\ H_{\text{in}}^{n,k+1} \end{bmatrix} = \begin{bmatrix} f_{\text{dep}}(G^{n,k}, H_{\text{in}}^{n,k}) \\ \eta_{\text{RC}} f_{\text{gain}}(G^{n,k}, H_{\text{in}}^{n,k}) \end{bmatrix} = \mathbf{f}_{\text{SP}} \left(\begin{bmatrix} G^{n,k} \\ H_{\text{in}}^{n,k} \end{bmatrix} \right), \quad (12)$$

whereby $G^{n,k}$ denotes the gain before the n -th pulse passes the laser medium for the k -th time. Therefore, the effect of N_{RT} successive round-trips is given by the iterated function $\mathbf{f}_{\text{MP}} = \mathbf{f}_{\text{SP}}^{(N_{\text{RT}})} = \mathbf{f}_{\text{SP}} \circ \dots \circ \mathbf{f}_{\text{SP}}$. Since the pump power is usually changing slowly compared to the repetition rate of the pulse source, it can be assumed that the pump power remains approximately constant for the time between two consecutive pulses, i.e., $P_{\text{pump}}(t) \approx p^n$ for $t \in [t^n, t^{n+1})$ with $t^{n+1} = t^n + \Delta t$. As a result, the initial gain of the $(n+1)$ -st pulse is given by

$$G^{n+1,1} = f_{\text{pump}} \left(\begin{bmatrix} 1 & 0 \end{bmatrix} \mathbf{f}_{\text{MP}} \left(\begin{bmatrix} G^{n,1} \\ H_{\text{in}}^n \end{bmatrix} \right), p^n \right). \quad (13)$$

Choosing the input variable $u^n = H_{\text{in}}^n$, the output variable $y^n = H_{\text{out}}^n$ and the state variable $x^n = G^{n,1}$, the pulse-to-pulse dynamics of the RA can be written as a nonlinear discrete-time dynamic system

$$x^{n+1} = f_{\text{pump}} \left(\begin{bmatrix} 1 & 0 \end{bmatrix} \mathbf{f}_{\text{MP}} \left(\begin{bmatrix} x^n \\ u^n \end{bmatrix} \right), p^n \right) = f(x^n, u^n, p^n) \quad (14a)$$

$$y^n = \frac{\eta_{\text{out}}}{\eta_{\text{RC}}} \begin{bmatrix} 0 & 1 \end{bmatrix} \mathbf{f}_{\text{MP}} \left(\begin{bmatrix} x^n \\ u^n \end{bmatrix} \right) = h(x^n, u^n), \quad (14b)$$

with the dynamic map f and the output map h . The corresponding initial condition x^0 is given by the initial population inversion $\Delta N^0(z)$ according to (5a). By integration of (1), the input variable can be expressed as a function of the adjustable loss of the AOM

as $u^n = \eta_{\text{AOM}}^n H_{\text{seed}}$. Since $0 \leq \eta_{\text{AOM}}^n \leq 1$, it follows that the system is subject to the input constraint

$$0 \leq u^n \leq \bar{u}, \quad (15)$$

with $\bar{u} = H_{\text{seed}}$. As a result, the pulse-to-pulse dynamics of RAs governed by the quite general space-dependent model of the gain medium (3) can still be captured by a simple scalar discrete-time dynamic system analogous to [7].

Apart from short transient operations during start-up or when switching to a different operating point, RAs are mainly run in steady-state operation. For a given constant input u^s and a stationary pump power p^s , the resulting steady state x^s is given by the nonlinear equation

$$x^s = f(x^s, u^s, p^s), \quad (16)$$

with the corresponding steady-state output

$$y^s = h(x^s, u^s). \quad (17)$$

Because of the one-dimensional state variable, the solution of the fixed-point equation (16) as well as the dynamics of the RA can be illustrated graphically as shown in Fig. 2 for different pump powers and round-trip numbers using the parameter values given in Table 1 and a 10 nJ seed pulse. As one would expect, the qualitative behavior of

Table 1. Parameter values for the simulation scenarios.

Symbol	Value	Unit	Symbol	Value	Unit
λ	1030×10^{-9}	m	λ_P	980×10^{-9}	m
A_B	50.27×10^{-6}	m ²	γ_{21}	416.66	s ⁻¹
σ	8.0×10^{-25}	m ²	σ_P	9.0×10^{-25}	m ²
f_0	0.9736	1	f_1	0.0264	1
f_2	0.9217	1	f_3	0.0783	1
N_{dop}	3.8×10^{26}	m ⁻³	L	6×10^{-3}	m
W_{seed}	10×10^{-9}	J	η_{RC}	0.8	1
η_{out}	0.9	1	f_{rep}	1×10^3	Hz

the dynamic map f is similar to the simpler model with neglected cavity losses in [7]. However, the neglected cavity losses influence the observed dynamics quite significantly for high values of x and are particularly relevant for the output map h , where the energy of the output pulses starts to decrease for high values of x as the net gain during the last round-trips in a highly saturated gain medium becomes less than one. As we will see in Section 3, this entails limitations on the control strategy. As noted above, the maxima of the steady-state output power $P_{\text{out}}^s = \frac{h\omega A_B}{\sigma(f_1+f_2)} f_{\text{rep}} y^s$ and the steady-state efficiency $\eta_{\text{eff}} = P_{\text{out}}^s / P_{\text{pump}}$ are usually inside or at the border of the unstable region, i.e., all x^s with $|\frac{\partial f}{\partial x}(x^s, u^s)| \geq 1$, as illustrated in Fig. 3.

3. Feedback stabilization of unstable operating regions

Building on the derived model above, we want to stabilize the dynamics of the RA by modulating the seed pulses based on some measured quantity of the amplifier. While using measurements of the output pulses y^n is probably the most obvious quantity, a simpler alternative is to use the transmitted pump light instead.

Since the pump power is usually not changed dynamically, but only adjusted to reach a desired operating point, we will utilize a so-called gain scheduling approach [18] in the following. Thereby, one determines a family of feedback laws for an arbitrary pump power

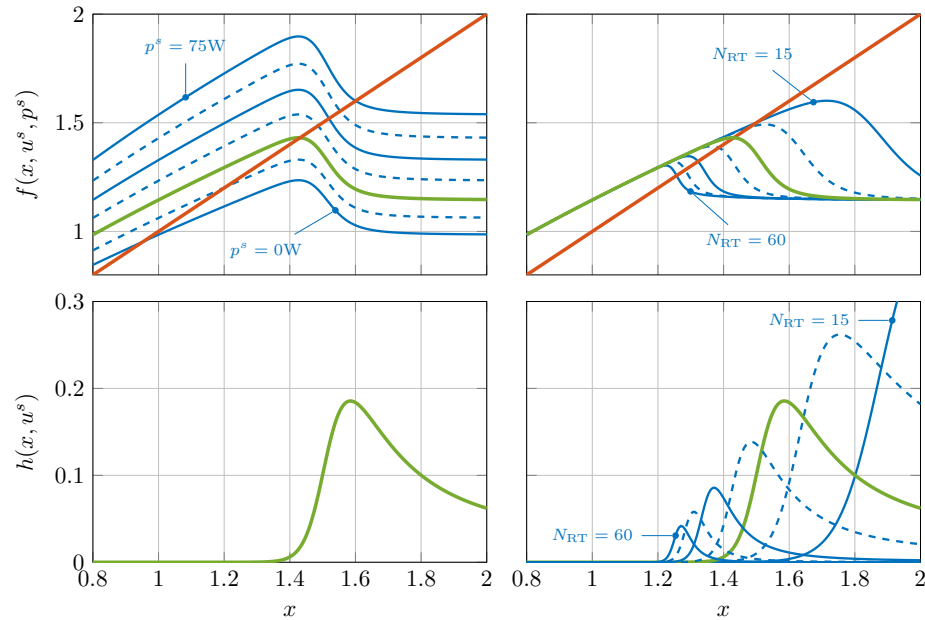


Fig. 2. Graphical illustration of the fixed-point equation (16) to obtain the steady state x^s (top) and the corresponding output equation for a given steady-state input u^s (bottom) for different stationary pump powers p^s and numbers of round-trips N_{RT} . On the left: Variable pump power $p^s \in \{0 \text{ W}, 12.5 \text{ W}, 25 \text{ W} \dots, 75 \text{ W}\}$ and $N_{RT} = 25$. On the right: Variable round-trips $N_{RT} \in \{15, 20, 25, 30, 40, 50, 60\}$ and $p^s = 25 \text{ W}$. The common case $N_{RT} = 25$ and $p^s = 25 \text{ W}$ is highlighted in green.

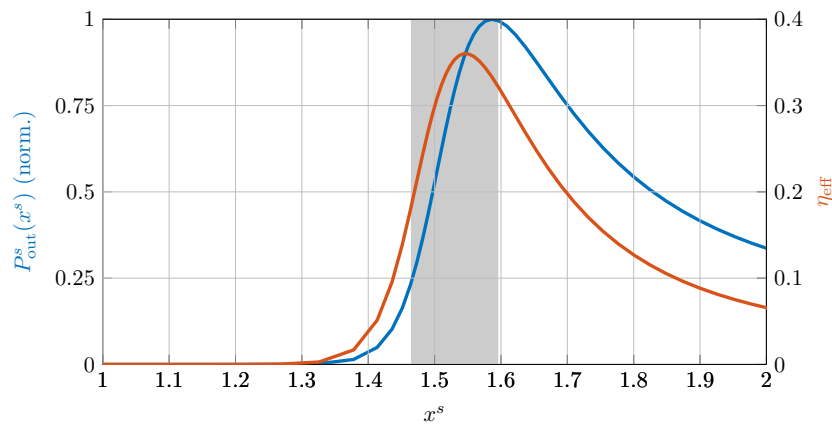


Fig. 3. Normalized steady-state output power P_{out}^s and steady-state efficiency η_{eff} as a function of x^s for $N_{RT} = 25$. The shaded area indicates unstable operating points.

p^s and switches between them during operation according to the current pump power. To simplify the design of a suitable feedback law, we linearize the system dynamics in the vicinity of an arbitrary operating point $(x^s(p^s), u^s)$, which is a solution of (16), to obtain a family of linear systems

$$\Delta x^{n+1} = \Phi(p^s) \Delta x^n + \Gamma(p^s) \Delta u^n \quad (18a)$$

$$\Delta y^n = C(p^s) \Delta x^n + D(p^s) \Delta u^n, \quad (18b)$$

with $\Delta u^n = u^n - u^s$, $\Delta x^n = x^n - x^s(p^s)$, and $\Delta y^n = y^n - y^s(p^s)$ as well as

$$\Phi(p) = \frac{\partial f}{\partial x}(x^s(p), u^s, p), \quad \Gamma(p) = \frac{\partial f}{\partial u}(x^s(p), u^s, p), \quad (19a)$$

$$C(p) = \frac{\partial h}{\partial x}(x^s(p), u^s), \quad D(p) = \frac{\partial h}{\partial u}(x^s(p), u^s), \quad (19b)$$

according to the Appendix. The choice of the steady-state input u^s is only restricted by the input constraint (15). While values close to $u^s = \bar{u}/2$ allow large control signals, lower input energies destabilize the natural behavior of the RA which is why steady-state inputs in the upper half of the possible range are typically preferred.

3.1. Feedback stabilization using pump light measurements

Like incoming laser pulses are amplified due to the population inversion in the laser medium, so is the light of the pumping beam absorbed. As a result, one can see fluctuations in the transmitted pump light due to the extraction and regeneration of the population inversion. Solving (9a) by separation of variables yields

$$\frac{I_P(L, t)}{I_0} = \left[\frac{G(t)}{G_{\max}} \right]^{\frac{\sigma_P(f_0+f_3)}{\sigma(f_1+f_2)^2}}, \quad (20)$$

with $G(t)$ according to (5a) and $G_{\max} = \exp\left(\sigma(f_1 + f_2) \frac{\kappa_1}{\kappa_2} LN_{\text{dop}}\right)$ denoting the gain at which the medium is transparent to the pumping beam. Since the state x^n is defined as the gain at time t^n just before the first round-trip of a pulse, one obtains

$$x^n = G_{\max} \left[\frac{I_P(L, t^n)}{I_0} \right]^{\frac{\sigma(f_1+f_2)^2}{\sigma_P(f_0+f_3)}}. \quad (21)$$

Thus, by measuring the transmitted light $I_P(L, t^n)$ we can directly infer the value of the system's state x^n . Together with the linearized behavior (18), the measured state according to (21) can then be used to design a state feedback law (see, e.g., [19])

$$u^n = g(x^n, p^n) = u^s + \varsigma(k_{\text{FB}}(p^n)(x^n - x^s(p^n))), \quad (22)$$

with the feedback gain $k_{\text{FB}}(p^n)$ and a strictly monotonous sigmoid function ς with $\varsigma(0) = 0$ and $\frac{d\varsigma}{du}(0) = 1$ to respect the input constraints (15). For example, when choosing $u^s = \bar{u}/2$ for a maximum of control headroom, i.e., setting the AOM at a steady-state level of $\eta_{\text{AOM}}^s = 1/2$, one can use

$$\varsigma(\xi) = (1 - \varepsilon)u^s \tanh\left(\frac{\xi}{(1 - \varepsilon)u^s}\right) \quad (23)$$

to obtain a smooth feedback law (22) where ε serves as a parameter to adjust the (relative) clearance towards both input constraints. Inserting the feedback law (22)

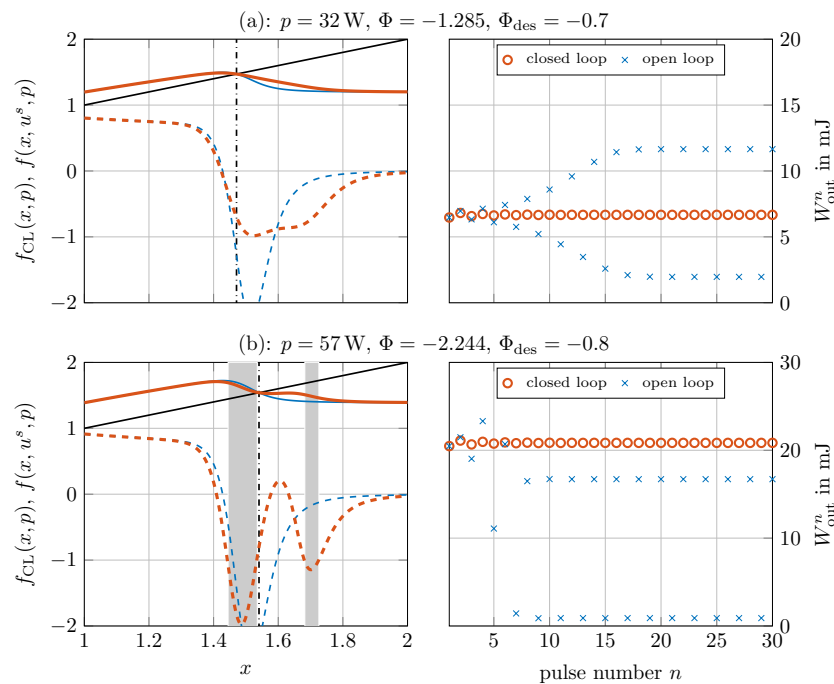


Fig. 4. Stabilization of a RA for two operating points. On the left: the closed-loop dynamics $f_{\text{CL}}(x, p)$ (solid) and its derivative $\frac{\partial f_{\text{CL}}}{\partial x}(x, p)$ (dashed) compared to the uncontrolled case. The shaded areas indicate regions where $\left| \frac{\partial f_{\text{CL}}}{\partial x}(x, p) \right| \geq 1$. On the right: the resulting sequence of output pulses W_{out}^n for $x^0 \approx x^s$.

into the dynamic system (14), one obtains the dynamics of the closed-loop system $f_{\text{CL}}(x^n, p^n) = f(x^n, g(x^n, p^n), p^n)$. Choosing the feedback gain as

$$k_{\text{FB}}(p) = \frac{\Phi_{\text{des}}(p) - \Phi(p)}{\Gamma(p)}, \quad (24)$$

the resulting linearized dynamics of the closed-loop system yields $\Delta x^{n+1} = \Phi_{\text{des}}(p^n) \Delta x^n$. Thus, the RA under feedback control is locally asymptotically stable at each operating point if $|\Phi_{\text{des}}(p)|$ is chosen smaller than one. As one can see in Fig. 4, the feedback law (22) locally modifies the dynamics of the RA such that the operating point due to the chosen pump power p is asymptotically stable (left-hand side). This is confirmed by numerical simulations using the full mathematical model (3) (right-hand side) illustrating the temporal evolution of the output pulse's energy $W_{\text{out}}^n = \frac{hA_B}{\sigma(f_1 + f_2)} y^n$ for an initial state x^0 close to the steady state x^s . Since the primary objective is to stabilize the RA, one only wants to change its natural dynamics if necessary, i.e., when $|\Phi(p)| \geq 1$. Including some safety margin, we choose

$$\Phi_{\text{des}}(p) = \begin{cases} \Phi(p) & \text{if } \Phi(p) > -0.9 \\ -0.9 & \text{otherwise.} \end{cases} \quad (25)$$

A simulation scenario for the given feedback law will be presented in Section 3.3.

3.2. Feedback stabilization using output energy measurements

While approaching the stabilization task by measuring the transmitted pump light is a simple and elegant method, such measurements are not always available, as for broadband pumping sources such as flash lamps or arc lamps. Additionally, if the energy of the amplified pulses are significantly below the capabilities of the gain medium, the fluctuation in the transmitted pumping beam may be too small to be measured reliably. In such cases, one can still follow the straightforward way to stabilize the regenerative amplifier using measurements of the pulse energy. Doing so will require to either infer the current state from output measurements by using state observers [19] or by applying some kind of output feedback. In the following, we will proceed along the latter path as it comes up with an easily implementable and computationally inexpensive control law by transforming (14) into a description based on input and output quantities only. In the vicinity of any x with $\frac{\partial h}{\partial x}(x, u) \neq 0$ there exists an inverse map $h^{-1}(y, u)$ such that $h(h^{-1}(y, u), u) = y$ for all u . Using this inverse map, the state dynamics (14) can be rewritten as

$$y^{n+1} = h(f(h^{-1}(y^n, u^n), u^n, p^n), u^{n+1}) = f_1(y^n, u^n, u^{n+1}, p^n). \quad (26)$$

Introducing the new state variable $\mathbf{z}^n = [y^n, u^n]^T$ and the new input $\nu^n = u^{n+1}$ yields the dynamically extended system model

$$\mathbf{z}^{n+1} = \begin{bmatrix} f_1(z_1^n, z_2^n, \nu^n, p^n) \\ \nu^n \end{bmatrix} = \mathbf{f}(\mathbf{z}^n, \nu^n, p^n). \quad (27)$$

Using $\Delta \mathbf{z}^n = [\Delta y^n, \Delta u^n]^T$ and $\Delta \nu^n = \nu^n - \nu^s$, one can linearize the extended system model at the steady state \mathbf{z}^s similar to (18), which yields

$$\Delta \mathbf{z}^{n+1} = \begin{bmatrix} \Phi & C\Gamma - \Phi D \\ 0 & 0 \end{bmatrix} \mathbf{z}^n + \begin{bmatrix} D \\ 1 \end{bmatrix} \Delta \nu^n = \Phi \mathbf{z}^n + \Gamma \Delta \nu^n, \quad (28)$$

with Φ , Γ , C , and D according to (33). The linearized system's dependence on p was omitted for brevity. Proceeding as in the previous subsection, a feedback law

$$\nu^n = \nu^s + \varsigma (\mathbf{k}_{\text{FB}}^T(p^n) \Delta \mathbf{z}^n) \quad (29)$$

can be used to stabilize the plant. The feedback gain $\mathbf{k}_{\text{FB}}^T(p) = [k_{\text{FB},1}(p), k_{\text{FB},2}(p)]$ can be determined using standard methods for linear systems such as pole placement or solving a discrete-time algebraic Riccati equation (DARE) as part of a linear quadratic regulator (LQR) problem [19]. Such solution strategies are possible for all p except for singular \tilde{p} where $C = \frac{\partial h}{\partial x}(x^s(\tilde{p}), u^s)$ vanishes (see Fig. 2). This is quite intuitive since one is not able to infer the system state x^n from output measurements in the vicinity of such points. While the singular points for $\tilde{p} = 0$ and $\tilde{p} \rightarrow \infty$ are irrelevant from a practical perspective, the singularity at the operating point with maximum output energy is more troublesome. Additionally, while a stabilizing solution \mathbf{k}_{FB} exists in the vicinity of \tilde{p} , the required feedback gains are usually very high which can be problematic to implement in the presence of measurement uncertainties and noise. As a result, feedback laws based on output measurements such as (29) are not suited to operate RAs in the vicinity of their maximum power output.

However, one is still able to pass through such singular points by limiting the resulting feedback gains in its vicinity and defining a region around \tilde{p} within which one interpolates

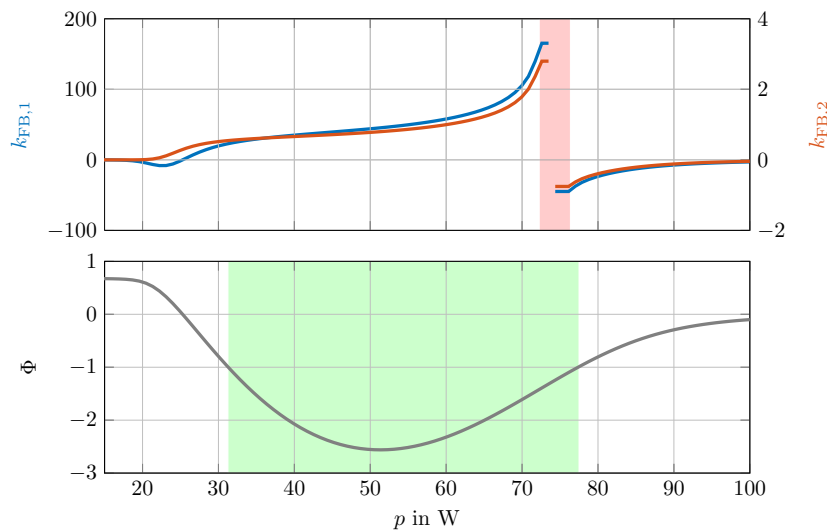


Fig. 5. A possible feedback gain $\mathbf{k}_{\text{FB}}(p)$ using an LQR formulation and a local interpolation around the singular point $\tilde{p} \approx 74$ W (shaded in red) compared to the linearized dynamics $\Phi(p)$ of the RA. Unstable operating points (i.e., $|\Phi| \geq 1$) are shaded in green.

between the values at the boundary in some sense. Assigning the nearest boundary values and using an LQR formulation as pointed out above, one obtains a feedback gain $\mathbf{k}_{\text{FB}}^T(p)$ illustrated in Fig. 5. Writing the control law with original variables, the output feedback law reads as

$$u^{n+1} = u^s + \varsigma \left(\mathbf{k}_{\text{FB}}^T(p^n) \begin{bmatrix} y^n - y^s(p^n) \\ u^n - u^s \end{bmatrix} \right). \quad (30)$$

The feedback law (30) is a dynamic system itself, whereby its linearized dynamics are determined by $k_{\text{FB},2}$. With this in mind, it is interesting to note that the LQR-based solution can result in control laws that are unstable on their own (i.e., $|k_{\text{FB},2}| > 1$, as in Fig. 5 for p approximately between 60 W and 74 W) but nevertheless yield a stable closed-loop dynamics when interconnected with the RA.

3.3. Simulation scenarios

The performance of the two feedback laws presented above shall be illustrated with simulation scenarios using the full mathematical model (3). To cover most of the interesting operational regimes of a regenerative amplifier, the optical pump power $P_{\text{pump}}(t)$ (and thus p^n) is chosen to start from a weakly pumped state at 12.5 W and increases linearly up to 87.5 W during the first 80 ms. After having passed the unstable regime completely, the amplifier is held at this highly pumped state for 40 ms, after which the pump power is decreased rapidly to 32.5 W within 15 ms and held there for the remaining time.

Fig. 6 shows simulation scenarios for both feedback laws in comparison to the uncontrolled open-loop case. In the uncontrolled case, small perturbations build up shortly after the amplifier enters the unstable regime while both feedback laws are able to successfully stabilize the amplifier and follow the desired steady-state output energies

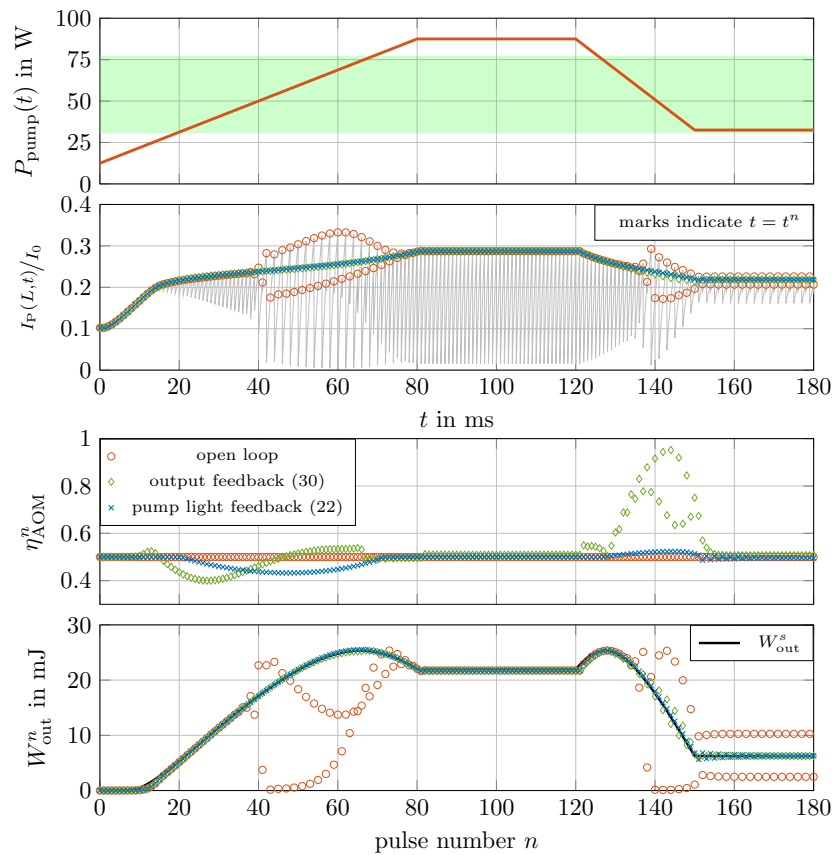


Fig. 6. Simulation scenario comparing an uncontrolled amplifier with a stabilized regenerative amplifier using the feedback laws (22) and (30) for a given trajectory of the optical pump power $P_{\text{pump}}(t)$ that passes the unstable region (shaded in green) twice. The continuous-time signal $I_P(t)$ (gray) corresponds to the open-loop case.

W_{out}^s . The comparatively slow increase in the pump power at the beginning elicits only minor corrective action by both feedback laws. However, the rapid decrease in pump power is fast enough to operate the output feedback law (30) close to its limits as indicated by the large input corrections necessary to keep the deviations of the output energy W_{out}^n close to the desired values. The availability of direct state measurements renders the feedback law (22) more robust to errors introduced by the gain scheduling approach. However, notice that the output feedback law (30) manages to keep the amplifier stable while passing through the singular pumping power \tilde{p} where the amplifier produces the highest possible output energies.

4. Experimental results

To demonstrate the effectiveness of the proposed feedback strategy in practice, it is applied to a Yb:CaF₂-based regenerative amplifier utilizing a linear cavity design with a double-pass pumping scheme which is seeded by 4 nJ pulses at $f_{\text{rep}} = 1$ kHz. By choosing $N_{\text{RT}} = 102$ (i.e., each pulse passes the gain medium 204 times due to the linear

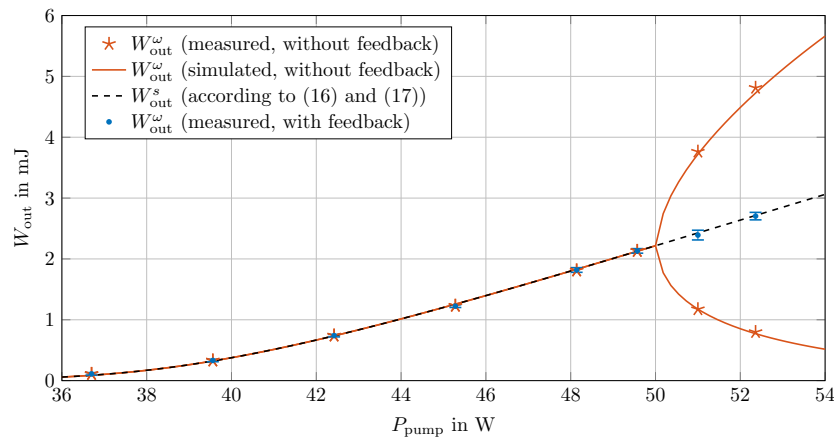


Fig. 7. Comparison of measured and simulated pulse energy values of the ω -limit set. Red indicates values without feedback, blue indicates values with feedback. While the amplifier becomes unstable for pump powers above $P_{\text{pump}} = 50$ W, the feedback law successfully stabilizes the output energies at the desired steady-state level W_{out}^s . The stabilized measurements include error bars to illustrate the standard deviation of the pulse energies.

cavity), one obtains an amplifier that allows sustained unstable operation at low power outputs without damaging the cavity optics by transient pulses. Due to the low energy extraction at such operating points, the fluctuations of the transmitted pump light are too small to be measured reliably. As a result, the feedback stabilization using pulse energy measurements presented in Section 3.2 is the only viable option.

The energy of the individual output pulses W_{out}^n is measured using a photo diode and observing the decay of the resulting voltage v_{ph} due to the parasitic resistances and capacitors. Since the photo current produced by the diode is proportional to the optical intensity, the jump height of the measured voltage signal is directly proportional to the energy of the incident laser pulse. Online estimates of the jump height can be obtained using polynomial or exponential least-squares approximations. In particular, least-squares techniques building on a discrete-time formulation of the underlying RC network compared favorable in terms of reliability and computational effort. As illustrated in Fig. 7, simulation results of the mathematical model (14) calibrated to the given setup (see, e.g., [20] for the relevant parameters of Yb:CaF2 crystals) agree very well with measurements of W_{out} . In particular, the model accurately predicts the energies of the ω -limit set W_{out}^{ω} for unstable operating points above $P_{\text{pump}} = 50$ W.

Since the gain-scheduled feedback law (30) is only a scalar dynamic system, it can be easily implemented on existing signal processing units. Notice that $\mathbf{k}_{\text{FB}}(p)$ and $y^s(p)$ can be calculated in advance for all p from the given system model and does not need to be computed online. Choosing $u^s = 0.7\bar{u}$ and applying the feedback law to the experimental setup, one is able to stabilize the regenerative amplifier and steer it into otherwise unstable operational regions. Unlike in the open-loop case, the feedback law suppresses the onset of bifurcations and keeps the output pulses W_{out}^n close to the desired steady-state energy W_{out}^s for a given pump power P_{pump} (see Fig. 7).

To illustrate the temporal effects of the feedback, we deactivate the feedback law by setting $u^n = u^s$ (i.e., $\eta_{\text{AOM}}^n = 0.7$) while operating the amplifier at $P_{\text{pump}} = 52.36$ W. Small perturbations start to build up immediately as shown in Fig. 8 (top) and the amplifier approaches the limit cycle W_{out}^{ω} again (cf. to Fig. 7). Details of the corresponding

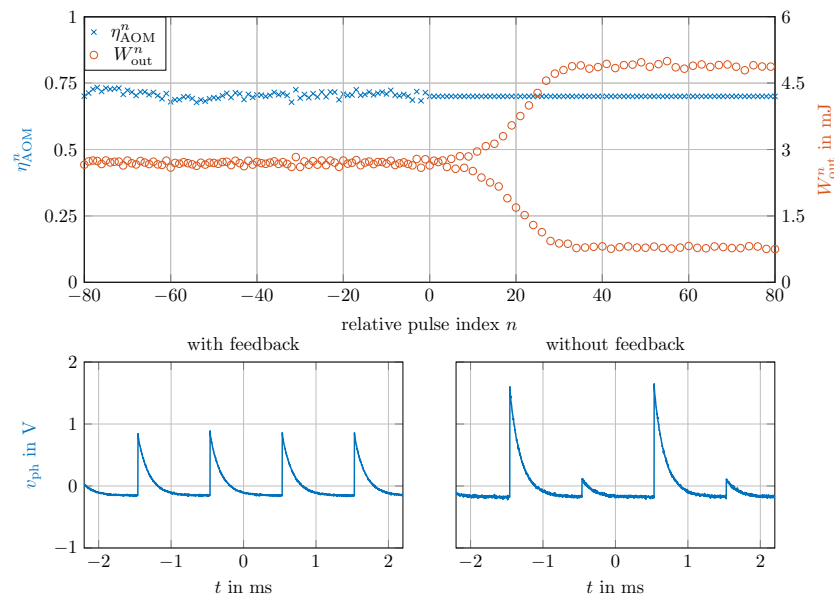


Fig. 8. Feedback-stabilized regenerative amplifier operated at $P_{\text{pump}} = 52.36 \text{ W}$ using the feedback law (30). For $n \geq 0$, the feedback is deactivated by setting $u^n = u^s$. As a result, small perturbations build up and the output pulse energy W_{out}^n approaches the limit cycle again. The corresponding voltages at the photo diode v_{ph} are illustrated at the bottom.

measured photo diode voltage $v_{\text{ph}}(t)$ are shown at the bottom of Fig. 8 for the case with and without feedback, respectively.

5. Conclusions and outlook

This paper demonstrates that unstable operational regimes and the resulting bifurcations of regenerative amplifiers can be suppressed by using feedback methods to actively modify the energy of incoming seed pulses. Starting from a general space-dependent mathematical description of the amplification and regeneration processes, it was shown that the dynamic behavior of RAs can be captured by a scalar discrete-time dynamic system under very mild assumptions only. Based on this dynamic model, two different control strategies were proposed using either output energy or transmitted pump light measurements. Both approaches are able to successfully stabilize RAs for general operating points. As a result, the utilization of feedback methods allows the operation of high-gain optical amplifiers without requiring multiple amplification stages to avoid bifurcations.

Using measurements of the output pulses entails limitations close to the operating point with maximum output energies as shown in Section 3.2. Nevertheless, it is possible to steer the amplifier through this singular point by traversing its vicinity fast enough while truncating the feedback gains. Those limitations do not apply to feedback approaches based on pump light measurements as presented in Section 3.1. Simulation studies furthermore show that such schemes are more robust due to the direct relation of the measurement to the system's state. However, the fluctuations of the transmitted pumping beam might be too small to obtain reliable measurements if the energy extracted by the amplification process is small compared to the stored energy. The choice between both

feedback schemes thus strongly depends on the specific properties of the given amplifier. To demonstrate the practical effectiveness of active feedback approaches, the output feedback scheme was successfully applied to a Yb:CaF₂-based RA.

Apart from stabilization purposes, altering the natural dynamics of RAs can be beneficial for the suppression of disturbances and to ensure a fast decay of perturbations to the steady state. Additionally, one could possibly apply similar feedback techniques to instabilities arising from the cavity dynamics in mode-locked cavity-dumped lasers [21]. While both feedback schemes presented in this thesis can be easily implemented on existing signal processing units, they rely on a mathematical model that is calibrated for the specific setup. Since the open-loop operation of unstable amplifiers close to their damage threshold is quite problematic, the development of closed-loop identification methods that can be performed online seems a promising direction for future investigations.

Appendix

Introducing the Jacobian of \mathbf{f}_{SP} with respect to x and u as

$$\nabla \mathbf{f}_{\text{SP}} \left(\begin{bmatrix} x \\ u \end{bmatrix} \right) = \begin{bmatrix} \frac{\partial \mathbf{f}_{\text{SP}}}{\partial x} & \frac{\partial \mathbf{f}_{\text{SP}}}{\partial u} \end{bmatrix} = \begin{bmatrix} \frac{e^{-u}}{\left((x-1)e^{-u}-x \right)^2} & \frac{x(x-1)e^{-u}}{\left((x-1)e^{-u}-x \right)^2} \\ \eta_{\text{RC}} \frac{e^u-1}{x(e^u-1)+1} & \eta_{\text{RC}} \frac{x e^u}{x(e^u-1)+1} \end{bmatrix}, \quad (31)$$

and the Jacobian of the iterated function \mathbf{f}_{MP} as

$$\begin{aligned} \nabla \mathbf{f}_{\text{MP}} \left(\begin{bmatrix} x \\ u \end{bmatrix} \right) &= \nabla \mathbf{f}_{\text{SP}} \left(\mathbf{f}_{\text{SP}}^{(N_{\text{RT}}-1)} \left(\begin{bmatrix} x \\ u \end{bmatrix} \right) \right) \times \nabla \mathbf{f}_{\text{SP}} \left(\mathbf{f}_{\text{SP}}^{(N_{\text{RT}}-2)} \left(\begin{bmatrix} x \\ u \end{bmatrix} \right) \right) \times \dots \\ &\quad \times \nabla \mathbf{f}_{\text{SP}} \left(\mathbf{f}_{\text{SP}} \left(\begin{bmatrix} x \\ u \end{bmatrix} \right) \right) \times \nabla \mathbf{f}_{\text{SP}} \left(\begin{bmatrix} x \\ u \end{bmatrix} \right), \end{aligned} \quad (32)$$

one obtains a linearized description of (14) according to (18) with

$$\begin{aligned} \Phi &= \frac{\partial f}{\partial x}(x^s, u^s) = \frac{df_{\text{pump}}}{dG_{\text{in}}} \left(\begin{bmatrix} 1 & 0 \end{bmatrix} \mathbf{f}_{\text{MP}} \left(\begin{bmatrix} x^s \\ u^s \end{bmatrix} \right) \right) \begin{bmatrix} 1 & 0 \end{bmatrix} \nabla \mathbf{f}_{\text{MP}} \left(\begin{bmatrix} x^s \\ u^s \end{bmatrix} \right) \begin{bmatrix} 1 \\ 0 \end{bmatrix} \\ \Gamma &= \frac{\partial f}{\partial u}(x^s, u^s) = \frac{df_{\text{pump}}}{dG_{\text{in}}} \left(\begin{bmatrix} 1 & 0 \end{bmatrix} \mathbf{f}_{\text{MP}} \left(\begin{bmatrix} x^s \\ u^s \end{bmatrix} \right) \right) \begin{bmatrix} 1 & 0 \end{bmatrix} \nabla \mathbf{f}_{\text{MP}} \left(\begin{bmatrix} x^s \\ u^s \end{bmatrix} \right) \begin{bmatrix} 0 \\ 1 \end{bmatrix} \\ C &= \frac{\partial h}{\partial x}(x^s, u^s) = \frac{\eta_{\text{out}}}{\eta_{\text{RC}}} \begin{bmatrix} 0 & 1 \end{bmatrix} \nabla \mathbf{f}_{\text{MP}} \left(\begin{bmatrix} x^s \\ u^s \end{bmatrix} \right) \begin{bmatrix} 1 \\ 0 \end{bmatrix} \\ D &= \frac{\partial h}{\partial u}(x^s, u^s) = \frac{\eta_{\text{out}}}{\eta_{\text{RC}}} \begin{bmatrix} 0 & 1 \end{bmatrix} \nabla \mathbf{f}_{\text{MP}} \left(\begin{bmatrix} x^s \\ u^s \end{bmatrix} \right) \begin{bmatrix} 0 \\ 1 \end{bmatrix}, \end{aligned} \quad (33)$$

where the dependence on the pump power p^s was omitted for clarity. Note that $f_{\text{pump}}(G_{\text{in}})$ denotes a solution of (10) with the initial condition $G(0) = G_{\text{in}}$. Since (10) is solved numerically, the derivative $\frac{df_{\text{pump}}}{dG_{\text{in}}}$ in (33) has to be approximated by some difference quotient, which requires the solution of (10) for two (or more) initial values.

Funding

Austrian Research Promotion Agency (859211); TU Wien University Library (Open Access Funding Programm)

Acknowledgments

The authors acknowledge the TU Wien University Library for financial support through its Open Access Funding Program.

Disclosure

The authors declare no conflicts of interest.

References

1. F. Krausz and M. Ivanov, "Attosecond physics," *Rev. Mod. Phys.* **81**, 163–234 (2009).
2. D. Goswami, "Optical pulse shaping approaches to coherent control," *Phys. Reports* **374**, 385–481 (2003).
3. S. Nolte, C. Momma, H. Jacobs, A. Tünnermann, B. N. Chichkov, B. Wellegehausen, and H. Welling, "Ablation of metals by ultrashort laser pulses," *J. Opt. Soc. Am. B* **14**, 2716–2722 (1997).
4. J. Dörring, A. Killi, U. Morgner, A. Lang, M. Lederer, and D. Kopf, "Period doubling and deterministic chaos in continuously pumped regenerative amplifiers," *Opt. Express* **12**, 1759–1768 (2004).
5. J. G. Mance, M. N. Slipchenko, and S. Roy, "Regenerative amplification and bifurcations in a burst-mode Nd:YAG laser," *Opt. Lett.* **40**, 5093–5096 (2015).
6. D. Mueller, A. Giesen, and H. Huegel, "Picosecond thin disk regenerative amplifier," in *14th International Symposium on Gas Flow, Chemical Lasers, and High-Power Lasers*, (Wroclaw, 2003), pp. 281–287.
7. M. Grishin, V. Gulbinas, and A. Michailovas, "Dynamics of high repetition rate regenerative amplifiers," *Opt. Express* **15**, 9434–9443 (2007).
8. M. Grishin, V. Gulbinas, and A. Michailovas, "Bifurcation suppression for stability improvement in Nd:YVO₄ regenerative amplifier," *Opt. Express* **17**, 15700–15708 (2009).
9. P. Kroetz, A. Ruehl, G. Chatterjee, A.-L. Calendron, K. Murari, H. Cankaya, P. Li, F. X. Kärtner, I. Hartl, and R. J. D. Miller, "Overcoming bifurcation instability in high-repetition-rate Ho:YLF regenerative amplifiers," *Opt. Lett.* **40**, 5427–5430 (2015).
10. L. von Grafenstein, M. Bock, G. Steinmeyer, U. Griebner, and T. Elsaesser, "Taming chaos: 16 mJ picosecond Ho:YLF regenerative amplifier with 0.7 kHz repetition rate," *Laser & Photonics Rev.* **10**, 123–130 (2016).
11. A. Efimov, M. D. Moores, N. M. Beach, J. L. Krause, and D. H. Reitze, "Adaptive control of pulse phase in a chirped-pulse amplifier," *Opt. letters* **23**, 1915–1917 (1998).
12. J. Prawiharjo, N. K. Daga, R. Geng, J. H. V. Price, D. C. Hanna, D. J. Richardson, and D. P. Shepherd, "High fidelity femtosecond pulses from an ultrafast fiber laser system via adaptive amplitude and phase pre-shaping," *Opt. Express* **16**, 15074–15089 (2008).
13. P. Malevich, G. Andriukaitis, T. Flöry, A. J. Verhoef, A. Fernández, S. Ališauskas, A. Pugžlys, A. Baltuška, L. H. Tan, C. F. Chua, and P. B. Phua, "High energy and average power femtosecond laser for driving mid-infrared optical parametric amplifiers," *Opt. Lett.* **38**, 2746–2749 (2013).
14. Y. Chiba, H. Takada, K. Torizuka, and K. Misawa, "65-fs Yb-doped fiber laser system with gain-narrowing compensation," *Opt. Express* **23**, 6809 (2015).
15. A. Deutschmann, P. Malevich, A. Baltuška, and A. Kugi, "Modeling and Iterative Pulse-Shape Control of Optical Chirped Pulse Amplifiers," *Automatica* **98**, 150–158 (2018).
16. L. M. Frantz and J. S. Nodvik, "Theory of Pulse Propagation in a Laser Amplifier," *J. Appl. Phys.* **34**, 2346–2349 (1963).
17. A. E. Siegman, *Lasers* (University Science Books, Mill Valley, 1986).
18. D. J. Leith and W. E. Leithead, "Survey of gain-scheduling analysis and design," *Int. J. Control.* **73**, 1001–1025 (2000).
19. T. Kailath, *Linear Systems*, Prentice-Hall Information and System Sciences Series (Prentice Hall, Upper Saddle River, NJ, 1980).
20. F. Druon, S. Ricaud, D. N. Papadopoulos, A. Pellegrina, P. Camy, J. L. Doualan, R. Moncorgé, A. Courjaud, E. Mottay, and P. Georges, "On Yb:CaF₂ and Yb:SrF₂: Review of spectroscopic and thermal properties and their impact on femtosecond and high power laser performance," *Opt. Mater. Express* **1**, 489–502 (2011).
21. M. S. Pshenichnikov, W. P. de Boeij, and D. A. Wiersma, "Generation of 13-fs, 5-MW pulses from a cavity-dumped Ti:sapphire laser," *Opt. Lett.* **19**, 572–574 (1994).